Chapter 7

Manganese-Zinc Spinel Ferrite Nanoparticles and Ferrofluids

Rajender Singh and Gadipelly Thirupathi

Additional information is available at the end of the chapter

http://dx.doi.org/10.5772/66522

Abstract

The nanoparticles and ferrofluids of spinel ferrites are useful in bio-sensors, transducers, storage devices, optical devices, and so on. The Mn-Zn ferrite (MZF) is generalized soft spinel ferrite having high saturation magnetization at low applied magnetic field. This chapter covers the synthesis of nanoparticles of various sizes and compositions of $Mn_{1-x}Zn_x$ Fe_2O_4 with x = 0–1 by co-precipitation method. The structural and magnetic properties of the nanoparticles are discussed. The ferrofluids of superparamagnetic and ferromagnetic MZF nanoparticles were synthesized. The magneto-viscosity of ferrofluids with the dispersion of nanoparticles in different colloidal was studied. The Herschel-Bulkley model is applied to analyse the data for low viscosity ferrofluids.

Keywords: spinel, Mn Zn ferrite, nanoparticles, ferrofluids

1. Introduction

Ferrites are ceramic materials with magnetic properties. According to the crystal structure, the ferrites are mainly classified as spinels, hexaferrites, garnets and perovskites. Spinel is the first class among these ferrites having mineral structure with significant magnetic behaviour. The nanoparticles and ferrofluids of spinel ferrites are useful in bio-sensors, transducers, storage devices, energy conversion devices, heat absorbers and generators, shock absorbers, lubricants, magneto-optical devices, and so on.

Among all ferrite types, the spinel ferrites are easy to form with control on the size of their nanoparticles. The Mn-Zn ferrite (MZF) is generalized soft spinel ferrite having high magnetization, and it saturates at low applied magnetic field. In this work, the optimization of the synthesis procedures was done to obtain stable nanoparticles and ferrofluids of Mn-Zn spinel ferrites. The structural and magnetic properties of the nanoparticles and magneto-viscosity of

the MZF ferrofluids were studied to understand the correlation between physical properties of nanoparticles and flow behaviour of ferrofluid in applied magnetic field.

2. Synthesis of nanoparticles of spinel ferrite

There are several methods for the synthesis of ferrite nanoparticles, that is, photo synthesis, microemulsion, sol-gel, hydrothermal, ball-milling, co-precipitation, catalyst-based methods and so on discussed in the literature [1–4].

In this work, the nanoparticles of $Mn_{1-x}Zn_x Fe_2O_4$ (MZF) with $x = 0$–1 were synthesized by soft chemical approach of co-precipitation method [5–10]. The metal salts with high solubility around room temperature, that is, $MnCl_2$, $ZnSO_4$ and $FeNO_3$, were chosen for the synthesis. The metal salts in stoichiometric mole ratio were dissolved in distilled water, and the mixture was heated at 353 K. The size of nanoparticles was controlled by controlling moles of OH^- ions in the solution (n) according to the following chemical formula:

$$(1\text{-}x)\ Mn^{2+} + x\ Zn^{2+} + 2\ Fe^{3+} + n\ OH^- \rightarrow Mn_{1-x}\ Zn_x\ Fe_2\ O_4 + H_2\ O$$

The solution was washed with distilled water until the pH = 7 was reached and the slurry was heated at 373 K to get the MZF nanoparticles. The MZF nanoparticles of different compositions in $Mn_{1-x}Zn_x Fe_2O_4$ with $x = 0$, 0.25, 0.5, 0.75 and 1 were synthesized.

3. Synthesis of the ferrofluids of spinel ferrite

The properties of ferrofluid depend on the hydrodynamic distribution of magnetic nanoparticles. The following ferrofluids were synthesized using MZF nanoparticles:

(i) Ferrofluids with the dispersion of superparamagnetic (SPM) nanoparticles (no surface coating) in ethylene glycol.

(ii) Ferrofluids with the dispersion of ferromagnetic nanoparticles in different colloidal with suitable surface coating of the nanoparticles.

Finding suitable colloidal is necessary for the stability of ferrofluid in various technological applications. A number of colloidal, with their properties listed in **Table 1**, were used for synthesizing different MZF ferrofluids using methods given the literature [11–15].

The synthesized (MZF) ferrofluids are listed in **Table 2**. These ferrofluids were studied for their magneto-viscosity properties. The table has three categories of ferrofluids:

(i) Ethylene glycol-based ferrofluids synthesized from SPM $Mn_{0.75}Zn_{0.25}Fe_2O_4$ nanoparticles.

(ii) Water, kerosene and toluene-based ferrofluids synthesized with surfactant-coated Mn-ferrite (MF) nanoparticles.

(iii) The ferrofluids synthesized with surfactant-coated $Mn_{0.75}Zn_{0.25}Fe_2O_4$ nanoparticles in water, kerosene, toluene and paraffin and $Mn_{0.9}Zn_{0.1}Fe_2O_4$ nanoparticles in paraffin.

S. No.	Colloidal	Dynamic viscosity of colloidal at 300 K (mPa. s)	Density (g/ml)	Vapour pressure (k Pa)
1	Ethylene glycol	16.2	1.1	0.5
2	Toluene	0.55	0.86	8.7
3	Kerosene	1.64	0.78	0.5
4	Water	0.8	1	4.3
5	Paraffin oil	25 to 80	1.1	0.5

Table 1. Properties of colloidal used for making ferrofluids.

Name of ferrofluid	Composition and magnetic behaviour of the nanoparticles	Colloidal	Surfactant
MZFE1	$Mn_{0.75}Zn_{0.25}Fe_2O_4$ (SPM)	Ethylene glycol	Not used
MFW	$MnFe_2O_4$ (FM)	Water	Tetra-methyl ammonia (TMA)
MFK		Kerosene	Oleic acid
MFT		Toluene	Oleic acid
MZFW	$Mn_{0.75}Zn_{0.25}Fe_2O_4$ (FM)	Water	TMA
MZFK		Kerosene	Oleic acid
MZFT		Toluene	Oleic acid
MZFP1		Paraffin oil	Oleic acid
MZFP2	$Mn_{0.9}Zn_{0.1}Fe_2O_4$ (FM)	Paraffin oil	Oleic acid

Table 2. Different MZF-based ferrofluids investigated in this work.

4. Structural and magnetic properties of spinel ferrites nanoparticles

The chemical formula of spinel ferrite is generally expressed, where 'Me' represents a divalent metal ion (e.g. Fe^{2+}, Ni^{2+}, Mn^{2+}, Mg^{2+}, Co^{2+}, Cu^{2+}, etc.) and '*i*' is inversion parameter which is 0 for normal spinel and 1 for inverse spinel. The inverse parameter varies from 0 to 1 for mixed spinel. The ionic radii of cation, crystal field effect, ionic charge, and so on are the main factors for the cation distribution in the nanoparticles of spinel ferrites. In the cubic close-packed arrangement of the spinel structure, the unit cell has 32 octahedral sites (B-site) and 64 tetrahedral sites (B-site), out of which only 16 octahedral sites and eight tetrahedral sites are occupied.

The Mn-Zn ferrite nanoparticles of various sizes and compositions were synthesized. Their structural properties were studied by X-ray diffraction (XRD) analysis. The morphological and microstructure of these nanoparticles was analysed using transmission electron microscopy (TEM). The magnetic properties of the nanoparticles were studied by measuring magnetization as a function of temperature and applied magnetic field, $M(T,H)$ and temperature-dependent ferromagnetic resonance (FMR) spectra.

The MZF nanoparticles of various sizes were synthesized by varying metal ions to hydroxide ratio (r = Me/OH^-) by co-precipitation method [16]. The value of r was varied from 0.375 to 0.17. The XRD patterns of all the samples (**Figure 1**, left) are analysed using Rietveld refinement method. The structural refinements are fitted with a single-phase spinel structure

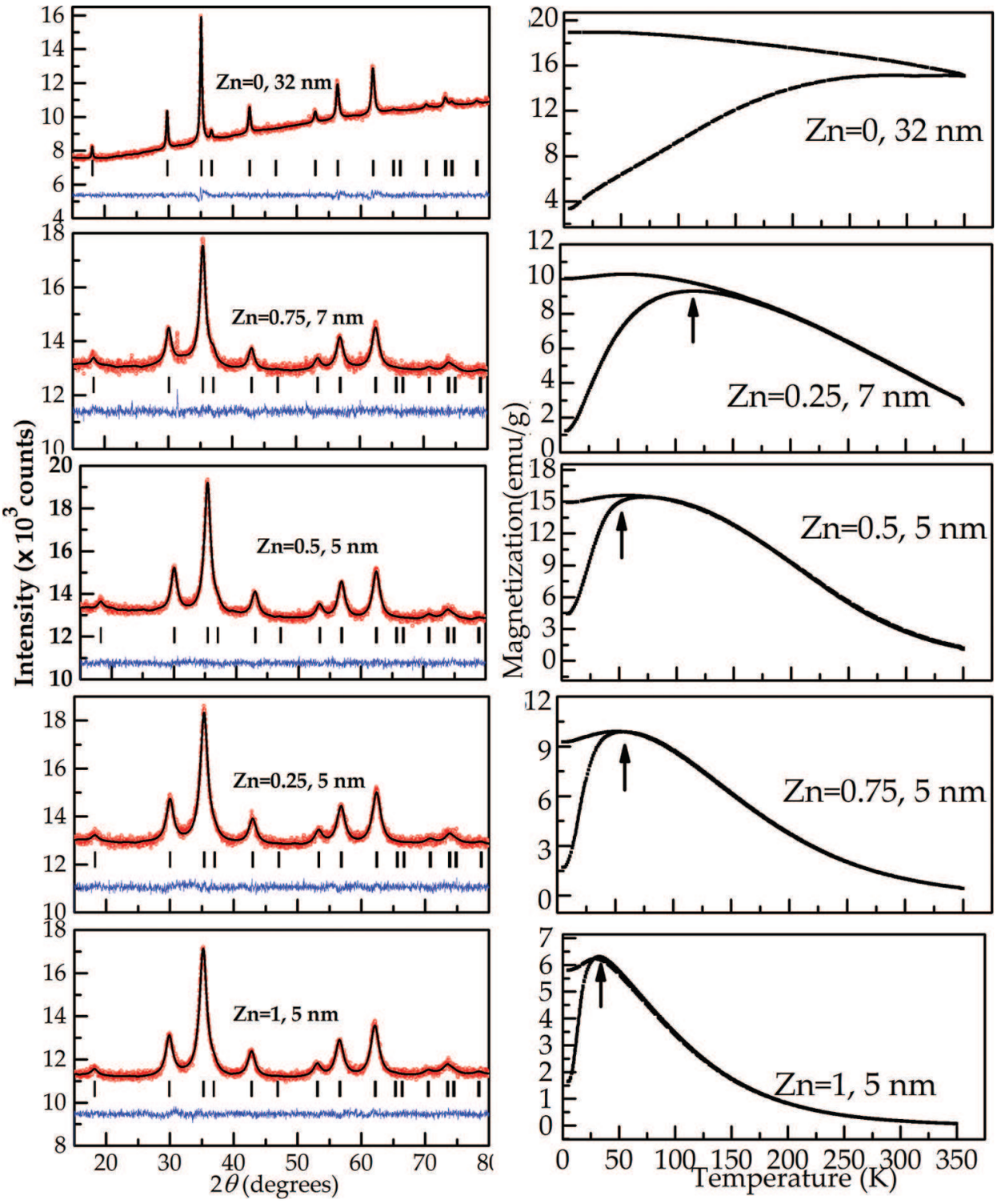

Figure 1. XRD pattern (left) and magnetization as a function of temperature at 100 Oe (right) of MZF nanoparticles for different Zn content.

Zn content	0		0.25		0.5		0.75		1	
S. No	D (nm)	a (Å)	D (nm)	a (Å)	D (nm)	a (Å)	D (nm)	a (Å)	D (nm)	a (Å)
1	32	8.483	7	8.411	4	8.418	3	8.439	2	8.461
2	60	8.478	10	8.427	5	8.410	4	8.431	5	8.451
3	104	8.477	11	8.412	7	8.397	5	8.419	9	8.447

Table 3. Listed here are lattice parameter (a) and crystallite size D determined from XRD for various compositions of $Mn_{1-x}Zn_x Fe_2O_4$ with $x = 0$–1 (MZF) nanoparticles.

having space group $Fd\bar{3}m$ by Fullprof suite program for the XRD pattern [17, 18]. The structural parameters (lattice parameter (a), crystallite size, strain, etc.) are extracted from the fits. The atomic position coordinates of A-, B- and O-sites are (1/8, 1/8, 1/8), (1/2, 1/2, 1/2) and (1/4+*u*, 1/4+*u*, 1/4+*u*), respectively. Here, *u* is the oxygen position coordinate shift parameter. The crystallite size and strain are calculated from Williamson-Hall plot for XRD pattern (see **Table 3**). Since the ionic radii of Mn^{2+} is comparable in coordination of octahedral and tetrahedral sites, so Mn-ferrite (MF) shows more inverse spinel ferrite.

The lattice parameter of MZF nanoparticles with $x = 0$, 0.5, 0.75 and 1 decreases with an increase in the size of the nanoparticle. This indicates the lattice contraction due to reduction of lattice disorder with an increase in nanoparticle size. The nanoparticles have several types of disorders such as oxygen deficiency, lattice disorders, dangling bonds, and so on. It is pointed out that the lattice expansion takes place with a decrease in nanoparticle size [19]. However, in the present study the lattice parameter of MZF nanoparticles with $x = 0.25$ increases initially when the particle size increases from 7 to 10 nm and then decreases with further increase in particle size. The nanoparticles of 7-nm size have impurity phase (Fe_3O_4 phase due to orthorhombic structure). The secondary impurity phase shares the lattice. So, the lattice parameter is lower for these nanoparticles. But in general, the resultant unit cell volume from both the phases will be higher.

The variation of crystallite size of MZF nanoparticles with Zn content is shown in **Figure 2** (left). The drastic decrease in crystallite size occurs at $x = 0.25$. This is attributed to the fact that when Zn^{2+} ions are substituted in Mn-ferrite, it causes a change from mixed spinel to normal spinel structure. The Zn^{2+} ions prefer to occupy tetrahedral site due to its stable valence

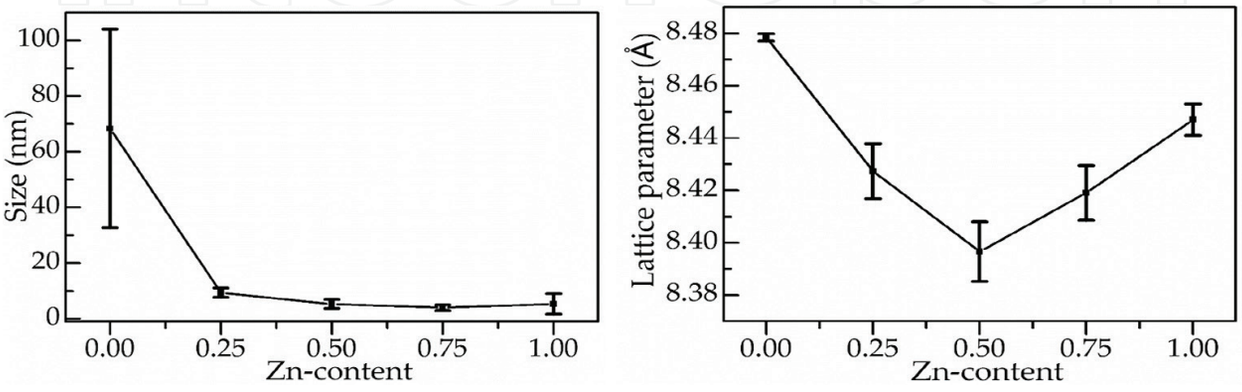

Figure 2. The variation of crystallite size (left) and lattice parameter (right) with Zn content of MZF nanoparticles.

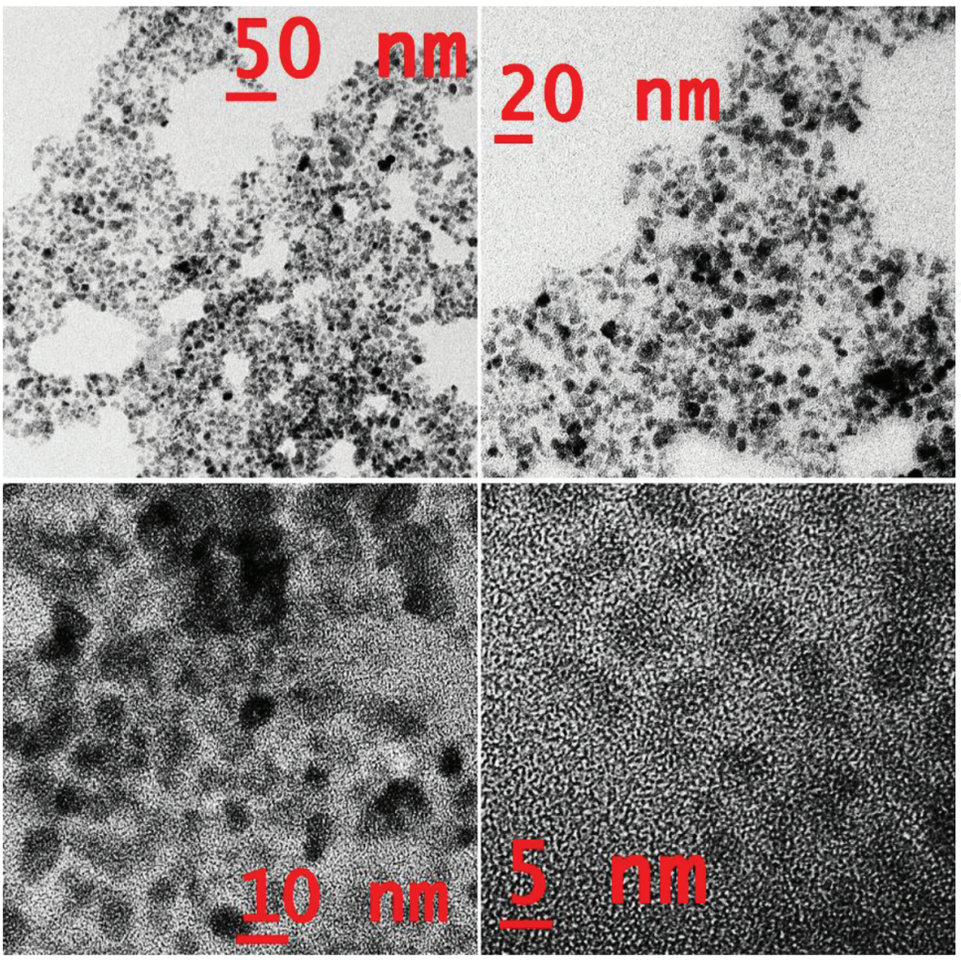

Figure 3. The TEM micrographs of $ZnFe_2O_4$ nanoparticles of crystallite size 5 nm.

and ion size. The decrease in crystallite size is marginal with further increase in Zn content. **Figure 3** (right) shows the variation of lattice parameter with Zn content in MZF nanoparticle. The lattice parameter decreases when x increases from 0 to 0.5 and then increases when Zn content increases from 0.5 to 1. This is due to the transition from mixed spinel to normal spinel phase as x increases from 0 to 0.5. The MZF nanoparticles again return to mixed spinel phase when x increases from 0.5 to 1. This is attributed to the nanophase formation due to the existence of lattice disorders in the system of nanoparticles.

The temperature dependence of the magnetization, $M(T)$, of Mn-ferrite and $Mn_{0.75}Zn_{0.25}Fe_2O_4$ nanoparticles measured at H = 100 Oe (see **Figure 1**, right) shows the bifurcation (irreversible) temperature (T_{irr}). The T_{irr}-value is high (>350 K) for Mn-ferrite nanoparticles. The irreversibility also depends on the crystalline size. The T_{irr} deceases when Zn content x = 0.25 is added in Mn-ferrite nanoparticles. This indicates the decrease in ferromagnetic interactions due to drastic decrease in size with Zn addition and the change in cation distribution which is influenced by the structural changes. With further increase in Zn content, the crystallite size becomes smaller than the critical superparamagnetic size. A single superparamagnetic particle or a system of mono-dispersed nanoparticles shows overlapped-blocking temperature (T_B) and irreversible temperature in $M(T)$ plots. If the size distribution of nanoparticles is taken

into account, each particle size will show a T_B-value. The resultant will be a distribution in T_B-value. The distribution of particle size and magnetic anisotropy is explained by thermomagnetic plots in earlier reports [20–22]. The T_B-value also depends on the magnetic field used for FC-ZFC mode and the measurement time. This is due to the slow relaxation of spins near the blocked state. The size distribution can be found from Neel's model. This model explains the relaxation of non-interacting single- domain nanoparticles experiencing uniaxial anisotropy. The uniaxial anisotropy gives a double well potential in two directions of spin alignment. The wells are separated by an energy barrier E_B to overcome thermal activation with the relaxation time [23]. The relaxation time is: $\tau = \tau_0 \exp(E_B/k_B T)$ whereas the $1/\tau_0$ is attempt frequency. In the small field limit: $E_B = K_{eff} V$ where the K_{eff} is the effective anisotropy constant and V is the particle volume. The volume distribution $f(V)$ can be estimated from M_{ZFC} plot (the thermomagnetic plot in zero-field-cooled mode). Then, the M_{ZFC} can be written in terms of distribution of $T_{B,}$ that is, $f(T_B)$ as follows:

$$m_{ZFC}(T) = \frac{H m_S^2(T)}{3 k_B T} \int_0^T f(T_B)\, d\, T_B$$

The equation implies to $f(T_B) \;\alpha\; \frac{d}{dT}(T\, m_{ZFC}(T))$

This equation is modified into the following by considering the log-normal size distribution $f(D)$ [21]:

$$f(D) \;=\; f_0(1/T_B^2)\frac{d}{dT}(T\, m_{ZFC}(T))$$

The decrease of T_B is observed in $M(T)$ plots of superparamagnetic MZF nanoparticles (**Figure 1**, right) with increase in Zn content from 0.5 to 1. This is due to the decrease in size and creation of short-range magnetic order in the nanoparticles. The T_B-value shift is attributed to the magnetic cluster formation and its size distribution [24–28]. The T_B-value and T_{irr} will overlap for the small-sized nanoparticles, whereas they are distinctly different for the large-sized particles. This is attributed to the existence of narrow-size distribution in the smaller nanoparticles compared to large nanoparticles [29–31]. The $M(T)$ results are in good agreement with the size distributions obtained from TEM data analysis. The uniform particle size distribution is observed in $ZnFe_2O_4$ nanoparticles of crystallite size 5 nm from the transmission electron microscope (TEM) micrograph analysis as shown in **Figure 3**.

Figure 4 (left) shows the magnetic hysteresis loops $M(H)$ plots of MZF nanoparticles at 5 and 325 K. These plots show soft ferrimagnetic behaviour for Mn-ferrite and $Mn_{0.75}Zn_{0.25}Fe_2O_4$ nanoparticles [32]. The coercivity is more for the $Mn_{0.75}Zn_{0.25}Fe_2O_4$ nanoparticles compared to Mn-ferrite at 5 and 325 K. This indicates that the domain size is more effective to slow domain wall motion in $Mn_{0.75}Zn_{0.25}Fe_2O_4$ nanoparticles due to non-magnetic Zn inclusion in Mn-ferrite. But there is not much change in saturation magnetization with $x = 0.25$ doping. Here, the surface-to-volume ratio plays more prominent role as the crystallite size decreases from 104 to 11 nm when Zn content varies from 0 to 0.25. Apart from this, Mn-ferrite is cubic spinel ferrite with a partial inverse spinel structure. Inter-sublattice super-exchange interactions of the cations on the (A–B) are much stronger than the (A–A) and (B–B) intra-sublattice exchange interactions. So, the cation distribution plays a major role on the magnetic properties of Mn-ferrite nanoparticles. The Zn

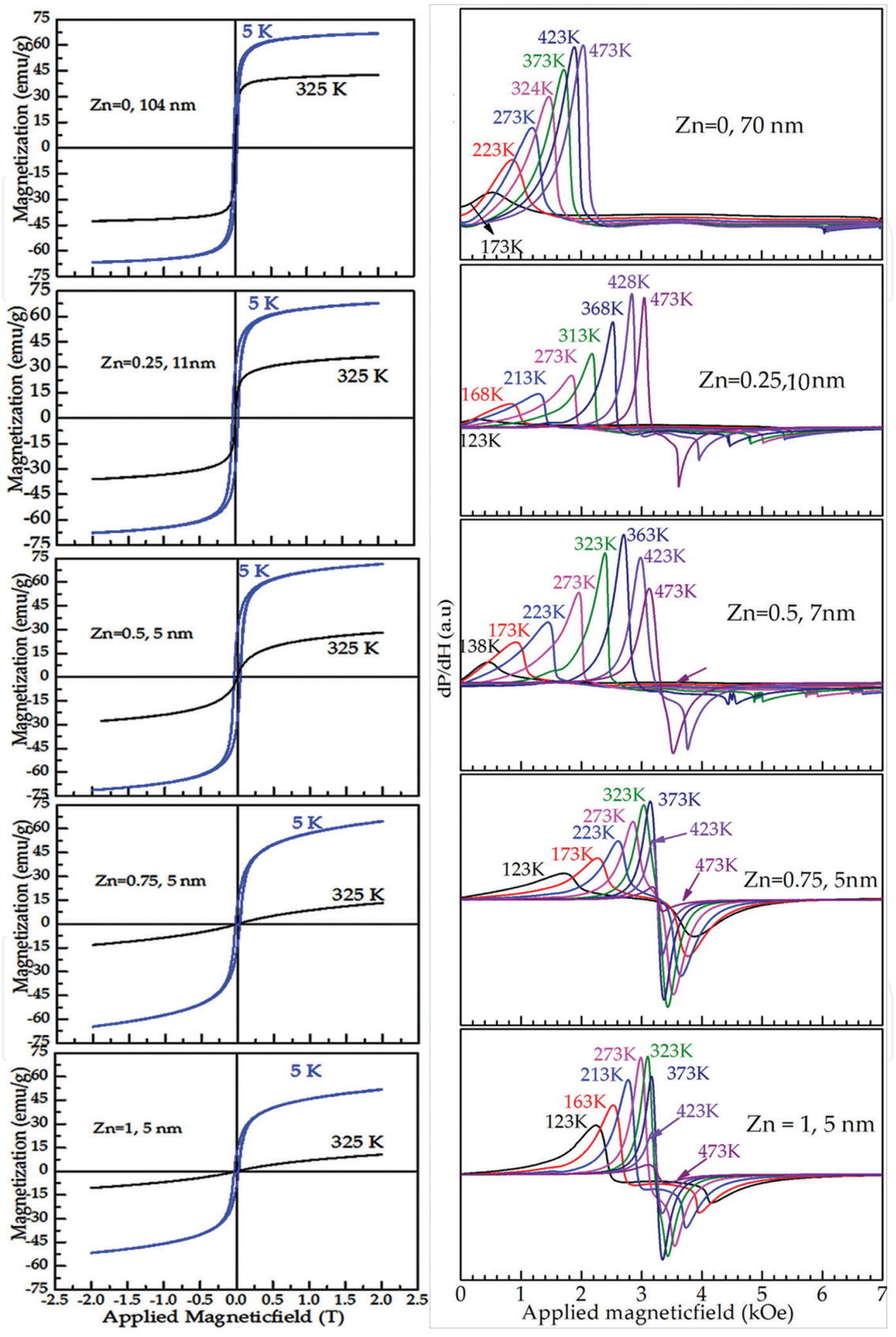

Figure 4. The M(H) plots at 5 and 325 K (left) and the FMR spectra (right) of MZF nanoparticles with different Zn content.

doping in Mn-ferrite decreases the crystallite size due to structural changes towards normal spinel structure. But the net magnetization is not reduced due to a decrease in the A-sublattice magnetization. So, the ferrimagnetism does not show much change in saturation magnetization.

The $M(H)$ plots of MZF nanoparticles with Zn content of 0.5, 0.75 and 1 having an average crystallite size of 5 nm show zero coercivity at 325 K and small coercivity at 5 K. This is because spins below blocking temperature do not relax. This can be attributed to spin canting and surface spin disorder in the nanoparticles [33, 34]. The coercivity at 5 K decreases with an increase in Zn content from 0.5 to 1. So, the decrease in blocking temperature can be expected with increasing Zn content. The shape of magnetization curve also depends on the measurement time and Neel relaxation of the nanoparticles. The $M(H)$ plots show the change in M_S which is due to the influence of the cationic stoichiometry and occupancy of cations in specific sites. In addition, random canting of particle surface spins and non-saturation effects due to a random distribution of particles are also responsible for the shape of $M(H)$ plots. The ferromagnetic resonance spectra shown in **Figure 4** (right) confirm the increase in the ferromagnetic component as Zn content is decreased in the MZF. This is indicated by progressive shifting of shoulder peak towards lower field value with a decrease in Zn content in MZF.

5. Investigation of magnetic properties of spinel ferrites based on Mössbauer studies

Mössbauer measurements on MZF nanoparticles were carried out at room temperature in transmission geometry using ^{57}Fe nuclei. Mössbauer spectrum of Mn-ferrite nanoparticles

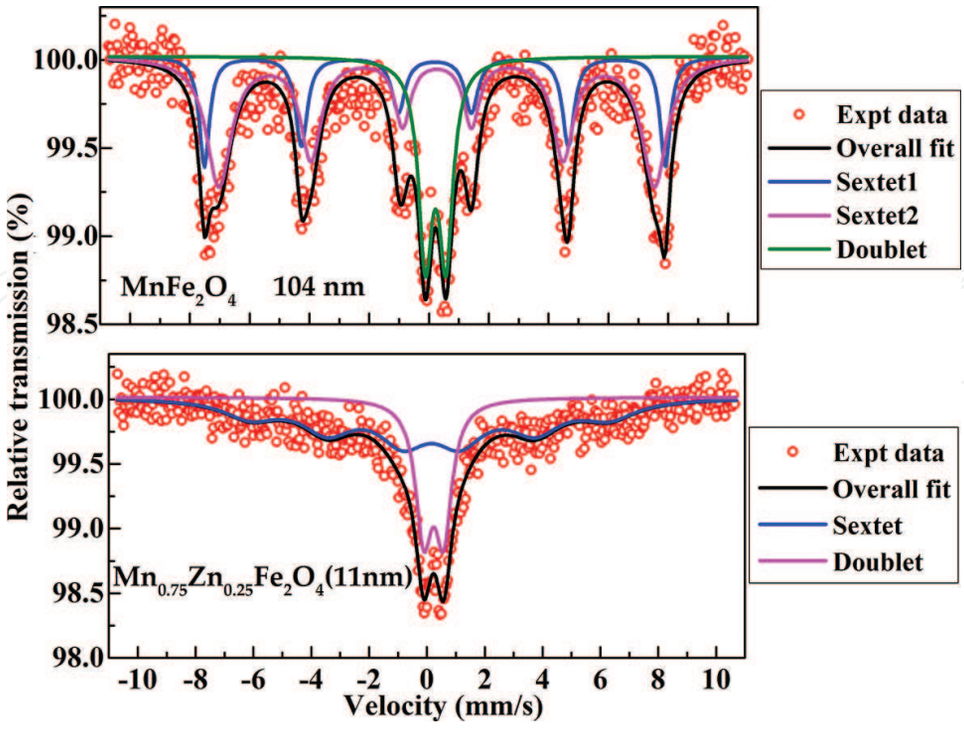

Figure 5. The Mössbauer spectra of Mn-ferrite and $Mn_{0.75}Zn_{0.25}Fe_2O_4$ nanoparticles.

with crystallite size of 104 nm is resolved into two sextets and one doublet (**Figure 5**). This system is soft ferromagnetic at room temperature. Two sextets come from two different Fe co-ordinations.

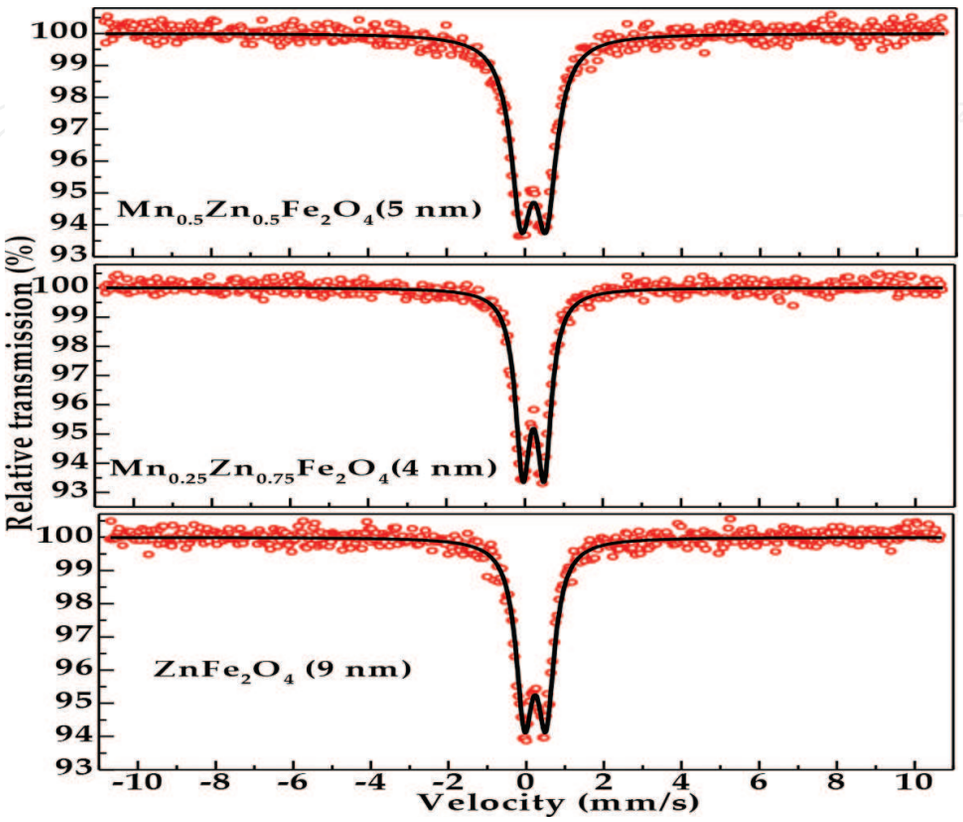

Figure 6. The Mössbauer spectra of MZF nanoparticles.

Sample	Sub-spectrum	Mössbauer parameters				
		H_{hf} (kOe)	Quadrupole shift (ΔE_q) (mm/s)	Isomer shift δ (mm/s)	Line width WV (mm/s)	Relative intensity (%)
$MnFe_2O_4$	Sextet-1 (A-site)	478	0.002	0.195	0.40	20
	Sextet-2 (B-site)	452	0.009	0.262	0.86	58
	Doublet (SPM)	–	0.691	0.223	0.55	22
$Mn_{0.75}Zn_{0.25}Fe_2O_4$	Sextet	385	0.055	0.129	1.86	67
	Doublet (SPM)	–	0.684	0.234	0.65	33
$Mn_{0.5}Zn_{0.5}Fe_2O_4$	Doublet (SPM)	–	0.633	0.222	0.65	100
$Mn_{0.25}Zn_{0.75}Fe_2O_4$	Doublet (SPM)	–	0.541	0.225	0.46	100
$ZnFe_2O_4$	Doublet (SPM)	–	0.553	0.231	0.53	100

Table 4. Parameters determined from the analysis of the Mössbauer spectra are listed here.

Sextet 1 has the hyperfine field value of 478 kOe and the absence of quadrupole splitting indicates that the Fe site is octahedral coordinated in cubic symmetry with 3+ valence state. Sextet 2 has a hyperfine field value of 452 kOe with quadrupole splitting of 0.009 mm/s due to 3+ valence state of Fe in tetrahedral coordination [35–37]. In addition, the doublet of relative area of around 22% is observed and this is due to the existence of small-sized magnetic particles showing superparamagnetic behaviour.

When 25 mole % of Zn (x = 0.25) is introduced in Mn-ferrite nanoparticles (with the crystallite size of 11 nm), the Mössbauer spectra are fitted with resolved one sextet and one doublet with a relative area of 67 and 33%, respectively. The sextet has a hyperfine field value of 385 Oe with quadrupole splitting of 0.055 mm/s. This indicates the possibility of tetrahedral coordination of Fe^{3+} ions. Mössbauer spectra of MZF nanoparticles (x = 0.5, 0.75 and 1) showed single-doublet pattern shown in **Figure 6** for the crystallite size of 5, 4 and 9 nm, respectively. This indicates that the nanoparticles are small-sized magnetic particles showing superparamagnetic behaviour at room temperature. Mössbauer parameters of all the samples investigated here are listed in **Table 4**.

6. Magneto-viscosity of ferrofluids of spinel ferrites

When the magnetic nanoparticles are suspended in colloidal, there are three main forces acting on the particles, that is, internal magnetic force, surface tension of the fluid and gravitational force. The ferrofluids show spikes when the fluid is subjected to the magnetic field. The chain-like or spot-like structure formation depends on these forces. The magneto-viscosity of the ferrofluid mainly depends on the magnetic properties of the nanoparticles used in the colloidal. The ferrofluids of superparamagnetic and ferromagnetic nanoparticles were chosen

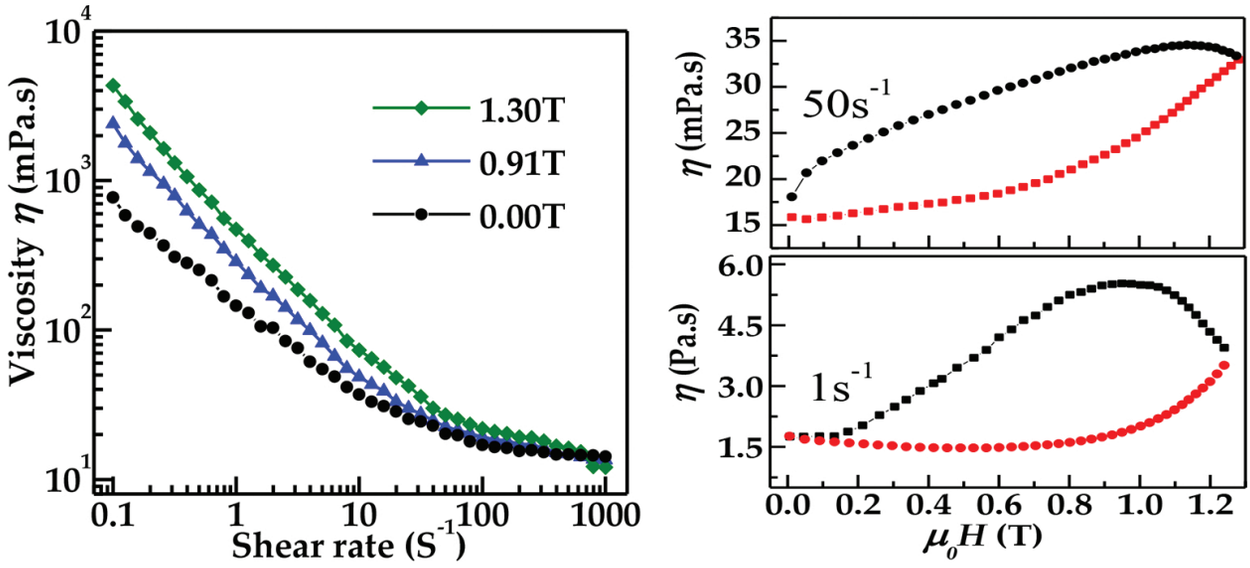

Figure 7. Flow curves at different applied fields (left) and magneto-viscosity curves at different shear rates (right) of MZFE ferrofluid.

for the study of magneto-viscosity. The surfactant coating to the nanoparticles increases the stability of the ferrofluid.

6.1. Magneto-viscosity of ferromagnetic nanoparticles-dispersed ferrofluid without surfactant coating

The $Mn_{0.75}Zn_{0.25}Fe_2O_4$ nanoparticles of 3-nm size were dispersed in ethylene glycol to prepare MZFE ferrofluid. The volume ratio of nanoparticles to the colloidal is 1:4. The superparamagnetic nature of the nanoparticles is confirmed by magnetization studies. **Figure 8** shows shear viscosity versus shear flow plot at various magnetic field values. The viscosity decreases with an increase in shear rate at zero magnetic field. It shows a shear-thinning effect at low shear rate and Newtonian behaviour over a wide range of shear rate. This can be explained by considering that at low shear rate the aggregates or clusters of nanoparticles offer high resistance to fluid flow leading to high viscosity. With increases in shear rate, the aggregates break into smaller units leading to fluid flow with low viscosity [38]. The interaction between aggregates or clusters increases when magnetic field is applied and aligns them in the direction of magnetic field forming chain-like structures which offer high resistance to the fluid flow leading to an increase in viscosity. Magneto-viscosity of other ferrofluids also shows similar behaviour [39, 40].

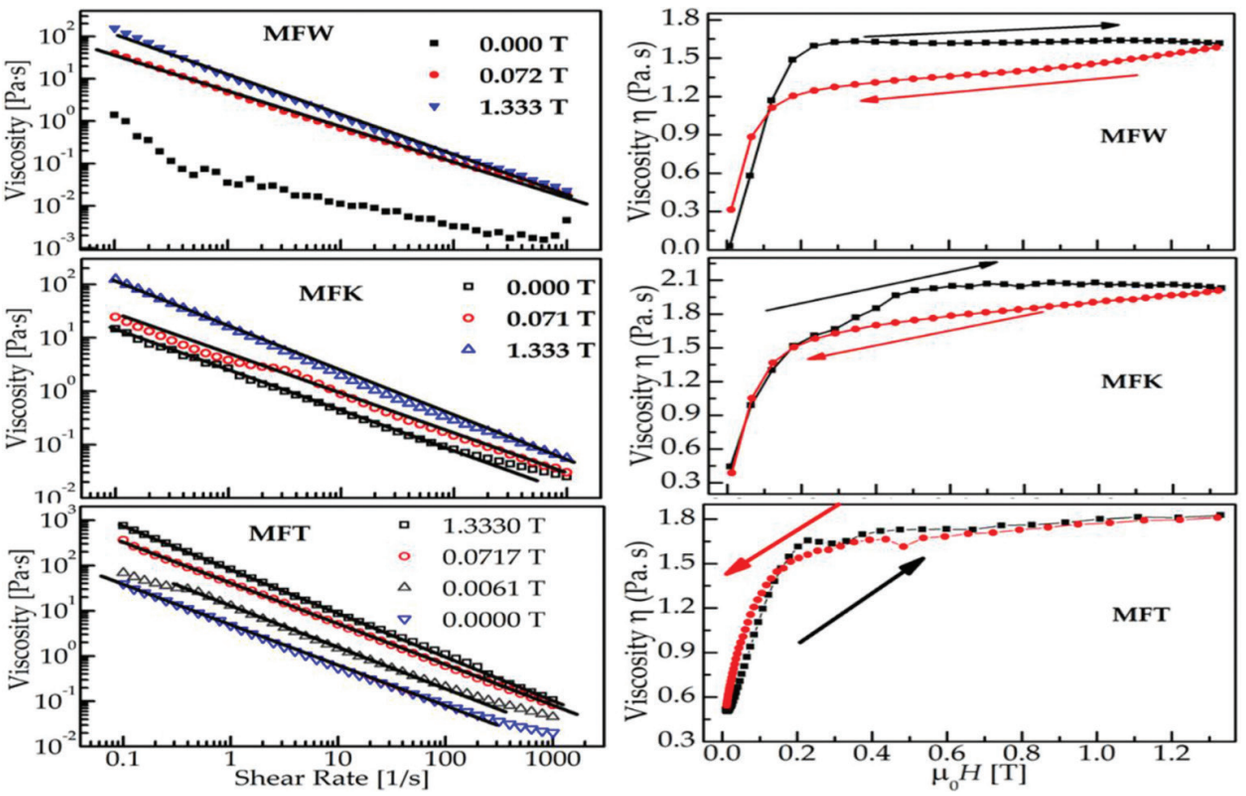

Figure 8. Viscosity as a function of shear rate at different applied magnetic fields (left) and viscosity as a function of applied magnetic field at a shear rate of 10 S^{-1} (right) of water-based (MFW), kerosene-based (MFK) and toluene-based (MFT) Mn-ferrite ferrofluids.

Odenbach [41] studied the magneto-viscous effect at various shear rates in a commercial magnetite-based ferrofluid and explained it in terms of interactions between the particles in the agglomerations aligned in straight chains and not due to the interaction between the chains. **Figure 7** shows irreversible nonlinear behaviour in η versus applied magnetic field plots at the steady shear rates of 1 and 50 s^{-1}. The irreversibility of magneto-viscosity curve is larger at low shear rate similar to the earlier reports [42]. The field dependence of viscosity indicates the particle size distribution and formation of chains with an increase in magnetic field. With a decrease in field, the viscosity increases due to the magnetic interactions and mechanical alignment of particles and slow loss of aggregation of particles. Then, the system tries to retain its initial state. The open hysteresis loop is due to unbroken chains and aggregates present in the system [43]. Odenbach [41] and Rhodesa [43] explained magnetic influence on the viscous properties of ferrofluid in terms of four forces acting on the magnetic particles in the ferrofluid. These forces arise from liquid media, internal magnetic field between magnetic particles, gravitational field and the applied magnetic field. The four regions in the plots of **Figure 7** are according to the limitations of these forces. Apart from this, the irreversibility is due to the relaxation of the nanoparticles in ferrofluids. The Brownian and Neel relaxations play a role for the observed behaviour of SPM nanoparticles in liquid media [13, 44].

6.2. Magneto-viscosity of surfactant-coated ferromagnetic nanoparticles-dispersed ferrofluids

It is quite interesting and more specific to study the magneto-viscosity of magnetic nanoparticles in less viscous colloidal such as water, kerosene and toluene. The ferromagnetic MF and MZF nanoparticles are used in different colloidal media with suitable surfactant coating for the preparation of MF and MZF ferrofluids. The surfactants have hydrophobic and hydrophilic ends. The hydrophilic end will be on the nanoparticle surface and hydrophobic end will overcome the formation of agglomerates of the nanoparticles. This property increases the stability of the ferrofluids.

6.2.1. Magneto-viscosity of Mn-ferrite ferrofluids

The magneto-viscosity of Mn-ferrite ferrofluid is investigated in flow field (flow curves) and in external magnetic field (magneto-viscosity plots). Mn-ferrite ferrofluids (i.e. MFW, MFK and MFT) were synthesized using Mn-ferrite nanoparticles suspension in different colloidal, that is, water, kerosene and toluene, respectively. The flow behaviour is studied for these ferrofluids in various applied magnetic fields. The respective volume ratio of Mn-ferrite nanoparticles, surfactant and colloidal (water, kerosene and toluene for respective ferrofluids) is taken as 1:0.5:1.5 for the preparation of Mn-ferrite ferrofluids. The MF nanoparticles are coated with tetramethyl ammonia (TMA) for the water-based MF ferrofluid (MFW). The kerosene-based ferrofluid (MFK) and toluene-based ferrofluid (MFT) are synthesized by using oleic acid-coated nanoparticles.

6.2.2. Flow curves of Mn-ferrite ferrofluids

Figure 8 (left) shows the flow curves of MF ferrofluid at various applied magnetic fields in the range from 0 to 1.33 T. The MFW ferrofluid shows non-Newtonian behaviour at lower shear

rates for zero magnetic field. The behaviour changes to Newtonian behaviour with increasing shear rate. The TMA coating of the nanoparticles exhibits more hydrophobic nature of the nanoparticles, leading to decrease in friction between the layers of the ferrofluid. So the power law behaviour cannot be observed in zero field magneto-viscosity plot for the water-based ferrofluid. For all the range of shear rates, it follows single behaviour, that is, power law behaviour without any discrepancy.

$$f(D) = f_0(1/T_B^2)\frac{\mathrm{d}}{\mathrm{dT}}(T\, m_{ZFC}(T))$$

Here, K is the consistency coefficient and the exponent n is the power law index.

Similar behaviour is observed in the MFK and MFT ferrofluids but the magnetic response is more. This is because the MFK and MFT are synthesized using FM nanoparticles in less viscous colloidal. So the hydrodynamic force is less compared to MFW ferrofluid. The very small n-value (0.1–0.05) indicates the high shear-thinning behaviour as reported in an earlier work [45]. With increase in applied field, n-value decreases indicating that the viscosity is affected more by magnetic field at low shear rates than at high shear rates [46, 47]. This is due to the competition between the flow field and the applied magnetic field. In this process, at higher shear rates (shear rate greater than 200 s^{-1}), the flow field dominates, whereas applied field dominates at lower shear rates. These ferrofluids showed completely non-Newtonian behaviour whereas the SPM nanoparticles-based ferrofluids (MZFE1) show the change in behaviour from non-Newtonian to Newtonian with an increase in shear rate similar to that reported in our earlier work [48, 49]. Above the applied field of 0.3 T, the magnetic nanoparticles (magnetic nano-dipoles) orient completely in the field direction with long-chain formation in the fluid.

6.2.3. Magneto-viscosity of Mn-ferrite ferrofluids

The magneto-viscosity plots at a shear rate of 10 s^{-1} (**Figure 8**, right) show a rapid increase with an increase in magnetic field initially, followed by its saturation at higher fields, with low hysteresis when the applied field is decreased to zero. Since the ferromagnetic particles are dispersed in less viscous fluid, as the field increases the nanoparticles try to rotate in the field direction [50–52]. Above the applied field of 0.3 T, the viscosity saturates. Because of long-chain formation along the field direction, the viscosity reaches the maximum possible value at the given shear rate. Magneto-viscosity at different shear rates is described in Refs. [53–56]. This behaviour is similar to magnetization plots of nanoparticles as a function of magnetic field.

6.2.4. Magneto-viscosity of Mn-Zn ferrite ferrofluids

Mn-Zn ferrite ferrofluids were synthesized using the MZF nanoparticles suspension in different colloidal, that is, water, kerosene, toluene and paraffin, respectively. The respective volume ratio of Mn-Zn ferrite nanoparticles, oleic acid and colloidal (water, kerosene, toluene or paraffin for respective ferrofluids) is taken as 1:0.5:1.5 for the preparation of Mn-Zn ferrite ferrofluids.

6.2.5. Flow curves of Mn-Zn ferrite ferrofluids

The flow behaviour is studied using flow curves shown in **Figure 9** (left)) for $Mn_{0.75}Zn_{0.25}Fe_2O_4$ ferrofluids in different applied magnetic fields. The fluid shows power law behaviour with

http://dx.doi.org/10.5772/66522

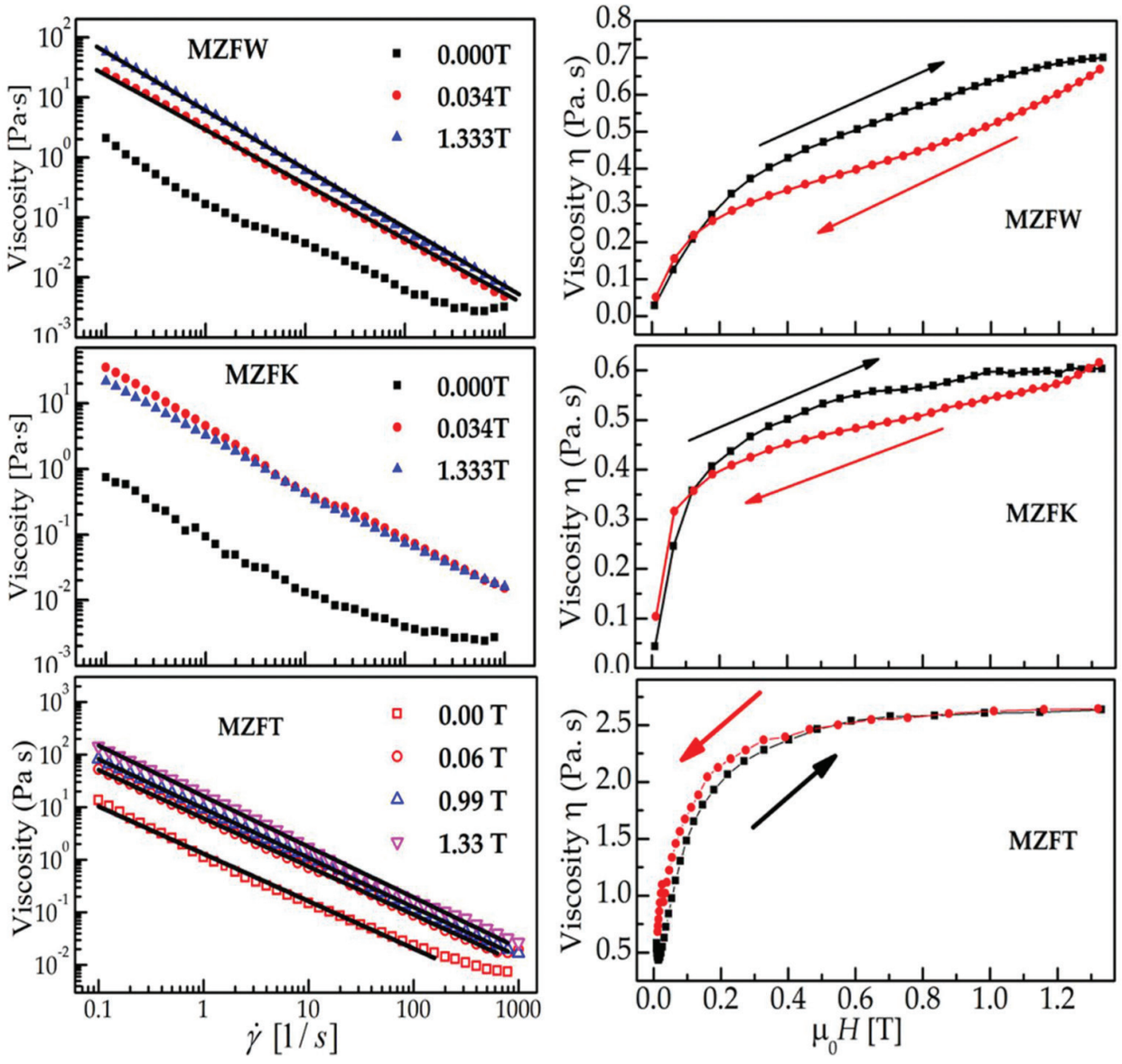

Figure 9. Viscosity as a function of shear rate at different applied magnetic fields (left) and viscosity as a function of applied magnetic field at a shear rate of 10 S^{-1} (right) of MZF ferrofluids synthesized with various colloidal.

small *n*-value between 0.1 and 0.04 for various magnetic fields in the range of 0–1.33 T indicating non-Newtonian behaviour with higher shear thinning [45]. The viscosity versus shear rate plot show the change from non-Newtonian to Newtonian behaviour at higher shear rates (shear rate greater than 300 s^{-1}), as we described in our earlier work [48]. The fluid viscosity behaviour is accounted to only the applied magnetic field. So for all the range of shear rate, it follows single power law behaviour without any discrepancy. The non-dimensional parameter, Mason number (*Ma*), explains the flow behaviour. Similar to electro-rheological fluids, the 'Ma' is the ratio of shear forces or hydrodynamic forces (F_H) to the magnetic forces (F_M), that is, $Ma = F_H/F_M$. The viscosity as a function of Mason number also follows the power law behaviour. The critical *Ma*-value determines the transition from magnetization to hydrodynamic control of the suspension structure [57].

6.2.6. Magneto-viscosity plots of Mn-Zn ferrite ferrofluids

The viscosity versus applied magnetic field at a shear rate of 10 S^{-1} is shown in **Figure 9** (right). The magneto-viscosity plots show a rapid increase with an increase in magnetic field initially. The viscosity is saturated at higher fields (around 0.2 T) and show low hysteresis when the applied field is decreased to zero. This behaviour is similar to the magnetization plots of the nanoparticles as a function of magnetic field.

6.2.7. Magneto-viscosity of paraffin-based ferrofluids

Paraffin is more stable colloidal compared with other colloidals used for the synthesis of ferrofluids. The dispersion of FM nanoparticles in paraffin gives fine control of viscosity in magnetic field. This study is quite interesting and useful for ferrofluid applications. Similar to the synthesis of other ferrofluids, the paraffin-based $Mn_{0.75}Zn_{0.25}Fe_2O_4$ (MZFP1) and $Mn_{0.9}Zn_{0.1}Fe_2O_4$ (MZFP2) ferrofluids are synthesized using oleic acid-coated nanoparticles. The magneto-viscosity plots of MZFP1 and MZFP2 ferrofluids are shown in **Figure 10** at the shear rate of 1 and 10 s^{-1}.

The comparison between the magneto-viscosity of these ferrofluids is as follows:

(i) The gradual increment of viscosity is observed in MZFP2 ferrofluid with an increase in magnetic field whereas sharp increment is observed in MZFP1 ferrofluid.

(ii) When the magnetic field is decreased, the magneto-viscosity plots of MZFP1 ferrofluid show less hysteresis and the plot is not relaxing to initial position at zero magnetic field.

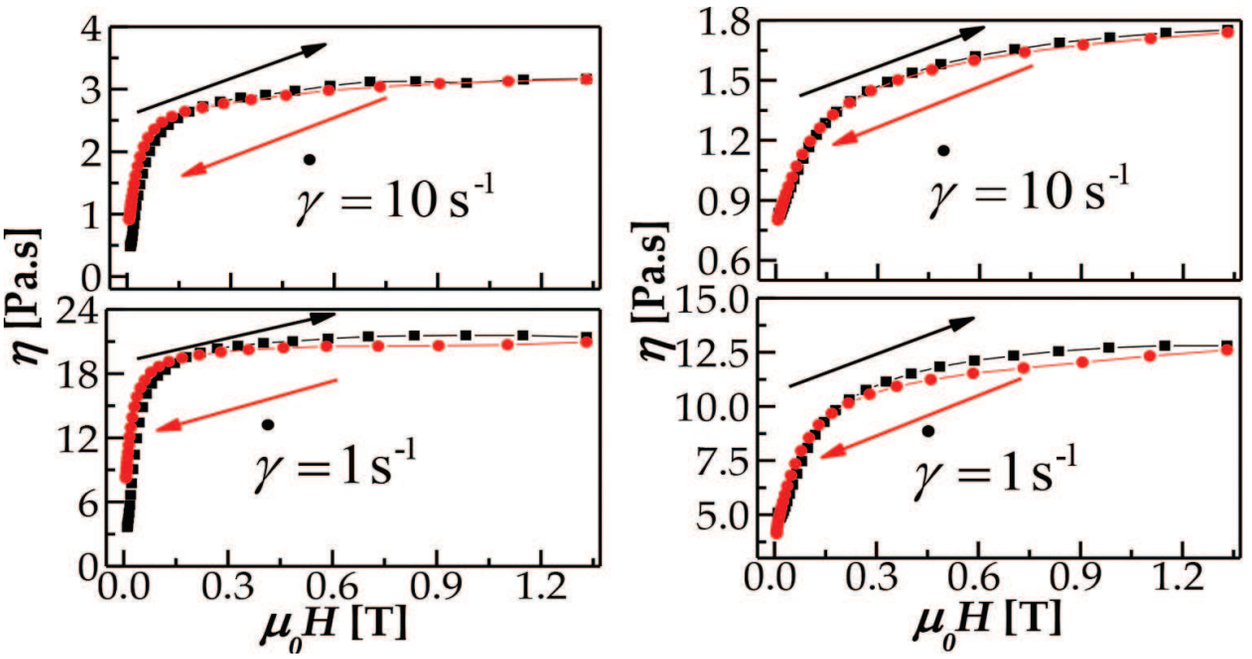

Figure 10. Viscosity as a function of applied magnetic field at different shear rates of paraffin-based ferrofluids of composition $Mn_{0.75}Zn_{0.25}Fe_2O_4$ (MZFP1) (left) and $Mn_{0.9}Zn_{0.1}Fe_2O_4$ (MZFP2) (right).

(iii) The magnetic nanoparticles are aligned in field direction and the nanoparticles are rotated along the easy axis of the system.

(iv) Resultant unbroken large chains are expected even when the magnetic field is removed. The MZFP2 ferrofluid shows different behaviour due to smaller-size particles and lower initial susceptibility.

6.2.8. The Herschel-Bulkley behaviour in ferrofluids

The MF nanoparticles dispersed in less viscous colloidal (toluene) are free to move in the fluid and so it is easy to study the structural changes in spot-like and chain-like structures as a function of applied magnetic field. MFT ferrofluid is chosen to explain the Herschel-Bulkley (H-B) behaviour in ferrofluids. Shear stress (τ) as a function of shear rate ($\dot{\gamma}$) plots is shown in **Figure 11**.

The H-B model combines the power law model with the yield stress as per the equation, $\tau = \tau_0 + K\dot{\gamma}^n$

Here, τ_0 is the yield stress. The yield stress can be determined from the plots using H-B model.

Apart from the magnetic behaviour of magnetic particles and the colloidal behaviour, the dosage of surfactant and the concentration of the magnetic nanoparticles in ferrofluids play a major role for the change of rheological behaviour at lower shear rates. This influences the flow field interaction in the ferrofluid. With the application of field, the shear stress versus shear rate plots show the H-B fluid behaviour. It is also observed as the magnetic field increases, the shear stress increases. The yield stress was determined by the extrapolation of the plots using the B-H model. The plots shifted upward due to the drastic change in yield stress. It increases from 4 to 27 Pa as magnetic field increases from 0 to 0.0717 T. The deviation from H-B model fit can be observed in shear stress (τ) versus shear rate plot at 1.33 T applied magnetic field [58]. As the applied field increases, the formation of chain-like and spot-like structure takes

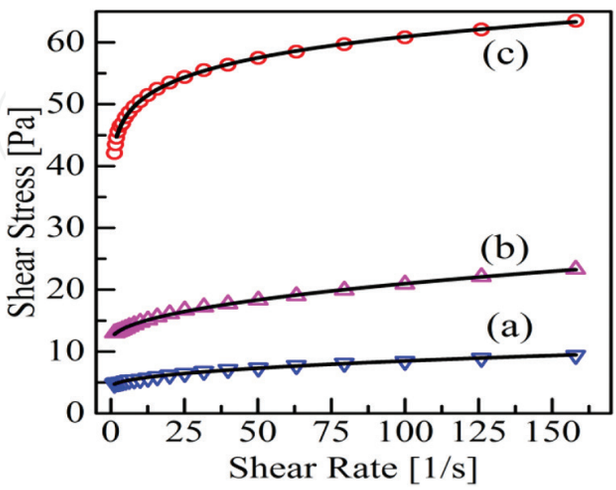

Figure 11. Shear stress as a function of shear rate, whereas solid line is H-B model fit for applied fields 0.000 (a), 0.0061 (b) and 0.0717 T (c) of MFT ferrofluid.

place [59]. The fluid remains as H-B fluid in the presence of small number of chains formed in the low field region with the increase in magnetic field. The strong- and long-chain formation occurs with the increase in magnetic field further. The magnetic field force dominates the other forces present in the fluid, as the magnetic field is increased leading to deviation from H-B fluid behaviour.

7. Conclusions

The nanoparticles of various sizes and compositions $Mn_{1-x}Zn_x Fe_2O_4$ with $x = 0–1$ were synthesized by co-precipitation method. The detailed structural and magnetic properties of MZF nanoparticles were carried out. The lattice parameter decreases with an increase in Zn content reaching a minimum value at $x = 0.5$ followed by an increasing trend with further increase in Zn content. The saturation magnetization and blocking temperature increase with a decrease in Zn content. The ferrofluids based on superparamagnetic and ferromagnetic MZF nanoparticles were synthesized. The magneto-viscosity of ferrofluids with the dispersion of nanoparticles in different colloidal was studied. The viscosity versus shear rate plot in applied magnetic field follows single power law behaviour without any discrepancy. The data on ferrofluids based on MF nanoparticles dispersed in less viscous colloidal (toluene) are analysed in view of Herschel-Bulkley model.

Author details

Rajender Singh* and Gadipelly Thirupathi

*Address all correspondence to: rsinghsp@gmail.com

School of Physics, University of Hyderabad, Hyderabad, India

References

[1] L. Yu, G. Hao, J. Gu, S. Zhou, N. Zhang, and W. Jiang, *Journal of Magnetism and Magnetic Materials*, vol. 394, pp. 14–21, Nov. 2015.

[2] J.-H. Yu, D.-W. Lee, B.-K. Kim, and T. Jang, *Journal of Magnetism and Magnetic Materials*, vol. 304, no. 1, pp. e16–e18, Sep. 2006.

[3] L. B. Tahar, H. Basti, F. Herbst, L. S. Smiri, J. P. Quisefit, N. Yaacoub, J. M. Grenèche, and S. Ammar, *Materials Research Bulletin*, vol. 47, no. 9, pp. 2590–2598, Sep. 2012.

[4] M. Staruch, D. Hires, D. Violette, D. Navarathne, G. A. Sotzing, and M. Jain, *Integrated Ferroelectrics*, vol. 131, no. 1, pp. 102–109, 2011.

[5] Y. Xuan, Q. Li, and G. Yang, *Journal of Magnetism and Magnetic Materials*, vol. 312, no. 2, pp. 464–469, May 2007.

[6] M. Sertkol, Y. Köseoğlu, A. Baykal, H. Kavas, and A. C. Başaran, *Journal of Magnetism and Magnetic Materials*, vol. 321, no. 3, pp. 157–162, Feb. 2009.

[7] R. Justin Joseyphus, A. Narayanasamy, K. Shinoda, B. Jeyadevan, and K. Tohji, *Journal of Physics and Chemistry of Solids*, vol. 67, no. 7, pp. 1510–1517, Jul. 2006.

[8] G. Thirupathi and R. Singh, *IEEE Transactions on Magnetics*, vol. 48, no. 11, pp. 3630–3633, Nov. 2012.

[9] R. M. Freire, T. S. Ribeiro, I. F. Vasconcelos, J. C. Denardin, E. B. Barros, G. Mele, L. Carbone, S. E. Mazzetto, and P. B. A. Fechine, *Journal of Nanoparticle Research*, vol. 15, p 2041, May 2013.

[10] K. Ali, A. K. Sarfraz, I. M. Mirza, A. Bahadur, S. Iqbal, and A. ul Haq, *Current Applied Physics*, vol. 15, no. 8, pp. 925–929, Aug. 2015.

[11] L. Vékás, M. V. Avdeev, and D. Bica, in *NanoScience in Biomedicine*, D. Shi, Ed. Springer: Berlin, Heidelberg, 2009, pp. 650–728.

[12] F. A. Tourinho, R. Franck, and R. Massart, *Journal of Material Science*, vol. 25, no. 7, pp. 3249–3254, Jul. 1990.

[13] I. Sharifi, H. Shokrollahi, and S. Amiri, *Journal of Magnetism and Magnetic Materials*, vol. 324, no. 6, pp. 903–915, Mar. 2012.

[14] N. Maleki-Jirsaraei, B. Ghane-Motlagh, F. Ghane-Golmohamadi, R. Ghane-Motlagh, and S. Rouhani, in *2010 International Conference on Nanoscience and Nanotechnology (ICONN)*, 2010, pp. 91–93.

[15] D. Maity and D. C. Agrawal, *Journal of Magnetism and Magnetic Materials*, vol. 308, no. 1, pp. 46–55, Jan. 2007.

[16] Z. X. Tang, C. M. Sorensen, K. J. Klabunde, and G. C. Hadjipanayis, *Journal of Applied Physics*, vol. 69, no. 8, pp. 5279–5281, Apr. 1991.

[17] E. Solano, C. Frontera, I. Puente Orench, T. Puig, X. Obradors, S. Ricart, and J. Ros, *Journal of Applied Crystallography*, vol. 47, no. 4, pp. 1478–1478, Aug. 2014.

[18] P. K. Manna, S. M. Yusuf, M. Basu, and T. Pal, *Journal of Physics: Condensed Matter*, vol. 23, no. 50, p. 506004, Dec. 2011.

[19] K. C. George, S. Kurien, and J. Mathew, *Journal of Nanoscience and Nanotechnology*, vol. 7, no. 6, pp. 2016–2019, Jun. 2007.

[20] B. D. Plouffe, D. K. Nagesha, R. S. DiPietro, S. Sridhar, D. Heiman, S. K. Murthy, and L. H. Lewis, *Journal of Magnetism and Magnetic Materials*, vol. 323, no. 17, pp. 2310–2317, Sep. 2011.

[21] R. S. DiPietro, H. G. Johnson, S. P. Bennett, T. J. Nummy, L. H. Lewis, and D. Heiman, *Applied Physics Letters*, vol. 98, no. 21, p. 216103, 2011.

[22] R. S. DiPietro, H. G. Johnson, S. P. Bennett, T. J. Nummy, L. H. Lewis, and D. Heiman, *Applied Physics Letters*, vol. 96, no. 22, p. 222506, 2010.

[23] A. Aharoni, *Introduction to the Theory of Ferromagnetism*. Oxford University Press, Great Clarendon Street, Oxford OX2 6DP ,2000.

[24] Q. Song and Z. J. Zhang, *Journal of Physical Chemistry B*, vol. 110, no. 23, pp. 11205–11209, Jun. 2006.

[25] P. Jeppson, R. Sailer, E. Jarabek, J. Sandstrom, B. Anderson, M. Bremer, D. G. Grier, D. L. Schulz, A. N. Caruso, S. A. Payne, P. Eames, M. Tondra, H. He, and D. B. Chrisey, *Journal of Applied Physics*, vol. 100, no. 11, p. 114324, Dec. 2006.

[26] K. Nadeem, H. Krenn, W. Sarwar, and M. Mumtaz, *Applied Surface Science*, vol. 288, pp. 677–681, Jan. 2014.

[27] K. Maaz, W. Khalid, A. Mumtaz, S. K. Hasanain, J. Liu, and J. L. Duan, *Physica E: Low-Dimensional Systems and Nanostructures*, vol. 41, no. 4, pp. 593–599, Feb. 2009.

[28] N. T. Lan, T. D. Hien, N. P. Duong, and D. V. Truong, *Journal of the Korean Physical Society*, vol. 52, no. 5, p. 1522, May 2008.

[29] Y. Jun, J. Seo, and J. Cheon, *Accounts of Chemical Research*, vol. 41, no. 2, pp. 179–189, Feb. 2008.

[30] M. Han, C. R. Vestal, and Z. J. Zhang, *Journal of Physical Chemistry B*, vol. 108, no. 2, pp. 583–587, Jan. 2004.

[31] S. Dey, S. K. Dey, B. Ghosh, P. Dasgupta, A. Poddar, V. R. Reddy, and S. Kumar, *Journal of Applied Physics*, vol. 114, no. 9, p. 093901, Sep. 2013.

[32] Q. Song and Z. J. Zhang, *Journal of the American Chemical Society*, vol. 134, no. 24, pp. 10182–10190, Jun. 2012.

[33] Rajshree B. Jotania and Hardev S. Virk, Ferrites and Ceramic Composites Trans Tech Publications,Inc, Reinhardstrasse 18, CH-8008 Zurich, Switzerland, 2013.

[34] S. Bedanta and W. Kleemann, *Journal of Physics D: Applied Physics*, vol. 42, no. 1, p. 013001, 2009.

[35] R. Malik, S. Annapoorni, S. Lamba, V. Raghavendra Reddy, A. Gupta, P. Sharma, and A. Inoue, *Journal of Magnetism and Magnetic Materials*, vol. 322, no. 23, pp. 3742–3747, Dec. 2010.

[36] L. B. Tahar, M. Artus, S. Ammar, L. S. Smiri, F. Herbst, M.-J. Vaulay, V. Richard, J.-M. Grenèche, F. Villain, and F. Fiévet, *Journal of Magnetism and Magnetic Materials*, vol. 320, no. 23, pp. 3242–3250, Dec. 2008.

[37] S. Kubickova, J. Vejpravova, P. Holec, and D. Niznansky, *Journal of Magnetism and Magnetic Materials*, vol. 334, pp. 102–106, May 2013.

[38] S. Odenbach and H. Störk, *Journal of Magnetism and Magnetic Materials*, vol. 183, no. 1–2, pp. 188–194, Mar. 1998.

[39] M. Chand, S. Kumar, A. Shankar, R. Porwal, and R. P. Pant, *Journal of Non-Crystalline Solids*, vol. 361, pp. 38–42, Feb. 2013.

[40] D. Soto-Aquino and C. Rinaldi, *Physical Review E*, vol. 82, no. 4, p 046310, Oct. 2010.

[41] S. Odenbach, *Colloids and Surfaces A: Physicochemical and Engineering Aspects*, vol. 217, no. 1–3, pp. 171–178, Apr. 2003.

[42] S. Odenbach, *Journal of Physics: Condensed Matter*, vol. 16, no. 32, pp. R1135–R1150, Aug. 2004.

[43] S. Rhodes, X. He, S. Elborai, S.-H. Lee, and M. Zahn, *Journal of Electrostatics*, vol. 64, no. 7–9, pp. 513–519, Jul. 2006.

[44] P. C. Fannin, L. Kinsella, and S. W. Charles, *Journal of Physics D: Applied Physics*, vol. 30, no. 4, p. 533, 1997.

[45] M. T. López-López, A. Gómez-Ramírez, L. Rodríguez-Arco, J. D. G. Durán, L. Iskakova, and A. Zubarev, *Langmuir*, vol. 28, no. 15, pp. 6232–6245, Apr. 2012.

[46] S. Odenbach, *Magnetoviscous Effects in Ferrofluids*. Springer: Berlin, 2002.

[47] K. Shah, R. V. Upadhyay, and V. K. Aswal, *Smart Materials and Structures*, vol. 21, no. 7, p. 075005, Jul. 2012.

[48] G. Thirupathi and R. Singh, *Physica B: Condensed Matter*, vol. 448, pp. 346–348, Sep. 2014.

[49] A. Y. Zubarev and L. Y. Iskakova, *Journal of Physics: Condensed Matter*, vol. 18, no. 38, p. S2771, Sep. 2006.

[50] L. J. Felicia and J. Philip, *Physical Review E*, vol. 89, no. 2, p. 022310, Feb. 2014.

[51] J. Nowak, E. Dohmen, and S. Odenbach, *IEEE Transactions on Magnetics*, vol. 50, no. 11, pp. 1–4, Nov. 2014.

[52] H. Shahnazian, D. Gräf, D. Y. Borin, and S. Odenbach, *Journal of Physics D: Applied Physics*, vol. 42, no. 20, p. 205004, Oct. 2009.

[53] A. Y. Zubarev and L. Y. Iskakova, *Physica A: Statistical Mechanics and Its Applications*, vol. 376, pp. 38–50, Mar. 2007.

[54] L. M. Pop and S. Odenbach, *Journal of Physics: Condensed Matter*, vol. 18, no. 38, p. S2785, Sep. 2006.

[55] D. Susan-Resiga and L. Vékás, *Rheologica Acta*, vol. 53, no. 8, pp. 645–653, Aug. 2014.

[56] K. Shah, R. V. Upadhyay, and V. K. Aswal, *Smart Materials and Structures*, vol. 21, no. 7, p. 075005, Jul. 2012.

[57] N. Gautam, G. Thirupathi, and R. Singh, *IEEE Transactions on Magnetics*, Article #: 4600204,Volume: 52, Issue: 7, July 2016

[58] R. Y. Hong, Z. Q. Ren, Y. P. Han, H. Z. Li, Y. Zheng, and J. Ding, *Chemical Engineering Science*, vol. 62, no. 21, pp. 5912–5924, Nov. 2007.

[59] M. Klokkenburg, B. H. Erné, A. Wiedenmann, A. V. Petukhov, and A. P. Philipse, *Physical Review E*, vol. 75, no. 5, p. 051408, May 2007.

IntechOpen